



Research articles

Non-cosine square angular-dependent magnetoresistance of the face-centered-cubic Co thin films

Yu Miao¹, Xiaorui Chen¹, Shuanglong Yang, Kun Zheng, Zhongyuan Lian, Yongzuo Wang, Pengju Wang, Cunxu Gao, De-Zheng Yang, De-Sheng Xue*

Key Laboratory for Magnetism and Magnetic Materials of the Ministry of Education, Lanzhou University, 730000 Lanzhou, PR China

ARTICLE INFO

Keywords:

Angular-dependent magnetoresistance
Small angle approximation
Cobalt

ABSTRACT

We found a non- $\cos^2\beta$ angular-dependent magnetoresistance (ADMR) of the face-centered-cubic Co thin films on MgO (001) substrates, where β is the angle between applied magnetic field \mathbf{H} and current I . Such angular dependence comes from the fact that the magnetization \mathbf{M} cannot be completely saturated in coherent rotation mechanism when \mathbf{H} deviates from the direction of easy and hard axes. By taking advantage of the Taylor's series, analytical expressions of the ADMR were derived for both out-of-plane and in-plane configuration. When H is larger than 2 times anisotropic field, the expressions can describe the magnetization-induced ADMR very well, where the maximum error at different angles is less than 5%. The non- $\cos^2\beta$ characteristic of the ADMR is helpful to distinguish the contribution of magnetization from others.

1. Introduction

The cosine square angular-dependent magnetoresistance (ADMR) is a character of the anisotropic magnetoresistance in ferromagnets [1–5] and the spin Hall magnetoresistance in heavy metal/ferromagnetic multilayers [6]. The cosine square characteristic of the ADMR has been used to confirm the presence of Dirac/Weyl fermions in Weyl semimetals [7,8], type-II Dirac semimetal VAl_3 [9] and NiTe_2 [10], as well as to reflect the twofold symmetry magnetoresistance from Fermi surface topology [11,12] in Bismuth [13] and semimetal LuPtBi [14]. When ferromagnetic materials contain two or more of the above physical mechanisms, such as in single ferromagnets induced spin current by itself [15] and magnetic Weyl semimetal $\text{Co}_3\text{Sn}_2\text{S}_2$ [16], it will be extremely useful to distinguish the ADMR induced by magnetization \mathbf{M} from other physical mechanisms.

The ADMR induced by \mathbf{M} is define as $\rho_{xx} = \rho_{\perp} + (\rho_{\parallel} - \rho_{\perp})\cos^2\varphi$ [17–20], where ρ_{\perp} and ρ_{\parallel} are the resistivities of the \mathbf{M} perpendicular and parallel to the current I , respectively, and φ is the angle between \mathbf{M} and I . If the formula is valid, it needs a hidden condition that amplitude of \mathbf{M} is an unchanged with determinable angles φ under the field \mathbf{H} . Alternatively, the ADMR can be expressed as

$$\rho_{xx} = \rho_{\perp} + (\rho_{\parallel} - \rho_{\perp})\cos^2(\beta - \alpha), \quad (1)$$

where β is the angle between \mathbf{H} and I , and α is the angle between \mathbf{M} and

\mathbf{H} . Experimentally, it is usually supposed that \mathbf{M} of magnetic materials is parallel to \mathbf{H} when the amplitude of \mathbf{H} is larger than the saturation magnetic field H_s [17]. In this situation $\alpha = 0$ and ρ_{xx} can be described as

$$\rho_{xx} = \rho_{\perp} + (\rho_{\parallel} - \rho_{\perp})\cos^2\beta. \quad (2)$$

Even if $H > H_s$, the orientation of \mathbf{M} is still dependent on \mathbf{H} except in spherical ferromagnets with completely disordered polycrystalline and magnetic domain composites.

Under an applied magnetic field, the magnetization can reverse through two mechanisms. One mechanism is domain wall nucleation and propagation [21], and the other is called coherent rotation, which can be well described by Stoner-Wolfarth model [22]. When the applied magnetic field is high enough such as over H_s , it can be ensured the coherent rotation of magnetization [23]. Then the magnitude of magnetization can be considered as a constant M_s , and the direction of \mathbf{M}_s under a rotated \mathbf{H}_s is described by the Stoner-Wolfarth model. However, even if \mathbf{H}_s is several times of the anisotropic field, the Stoner-Wolfarth model [22] indicates the magnetization can never be completely magnetized to the direction of \mathbf{H}_s except at the easy and hard axes. The supposition used in Eq. (2) that \mathbf{M}_s is parallel to the \mathbf{H}_s , is no longer valid, and the deviation of the $\cos^2\beta$ ADMR induced by \mathbf{M} is significant [24].

Here, we investigated the ADMR induced by \mathbf{M} in face-centered-

* Corresponding author.

E-mail addresses: yangdzh@lzu.edu.cn (D.-Z. Yang), xueds@lzu.edu.cn (D.-S. Xue).¹ Yu Miao and Xiaorui Chen contributed equally to this work.

cubic (fcc) Co single-crystal thin films on the MgO (001) substrates under room temperature. The samples can be approximately considered as single domain structure with cubic anisotropy when $H > H_s$. We found the non- $\cos^2\beta$ ADMR both in out-of-plane and in-plane geometry. This contrasts with the fact that H_s could magnetize the Co thin films in saturation state within the traditional point of view. Considering the direction derivation of \mathbf{M}_s from \mathbf{H}_s , a proper analytical expression was proposed to describe the ADMR induced by \mathbf{M} when the field H is larger than 2 times anisotropic field H_a . Similar to the single crystal Co thin films, the findings were further verified by the ADMR in polycrystalline Fe₂₀Ni₈₀ thin films. Such non- $\cos^2\beta$ ADMR can be considered as a character of the ADMR induced by \mathbf{M} .

2. Experimental

The 30-nm-thick Co thin films were prepared on polished MgO (001) single crystal substrates by using a molecular beam epitaxy system under a base pressure lower than 5×10^{-7} Pa. The substrates were outgassed up to 500 °C and kept at 300 °C for the steady deposition of fcc Co [25–27]. The deposition rate was kept constant at 1.01 Å/min. The 84-nm-thick Fe₂₀Ni₈₀ thin films were deposited on Si substrates at room temperature by radio frequency magnetron sputtering. An in-plane uniaxial magnetic anisotropy was induced by oblique deposition. The base vacuum was 7.5×10^{-5} Pa, the sputtering power was 80 W, the flow of Ar was 10 SCCM, and the sputtering pressure was 0.25 Pa.

The structure of Co thin film was characterized by high resolution x-ray diffraction (X'Pert MRD). The in-plane and out-of-plane hysteresis loops were obtained by VersaLab and superconducting quantum interference device magnetometer, respectively. The ADMR was measured by the Physical Property Measurement System equipped with a motorized sample rotator. All measurements are performed at room temperature. The schematic diagram of the ADMR measurement was shown in Fig. 1(a). The current is along x direction, the [110] direction of the Co thin films, which is the easy axis in-plane. We rotated magnetic field in both xy and xz planes, where α (β) is the angle between \mathbf{H} and \mathbf{M} (I).

3. Results and discussion

3.1. Structural and magnetic characterizations

Fig. 1(b) shows clear (002) diffraction peak of the Co thin film in the x-ray diffraction pattern, and there are no other impurity peaks, indicating the fcc structure of the crystal. Its in-plane hysteresis loops were shown in Fig. 1(c). The loop measured in the easy axis direction has a reduced remanence ~ 1.0 , which indicates that the sample is a single domain structure. With a decreasing field, the loop measured in the hard axis direction has a reduced remanence ~ 0.7 , which reveals that the in-plane magnetization process is a coherent rotation mechanism. To describe the deviation of \mathbf{M}_s from \mathbf{H} , we considered the Zeeman energy and the cubic magnetocrystalline anisotropy energy characterized by a constant K_{in} , the in-plane free energy density [17,28] is written as

$$F_{in} = -\mu_0 M_s H \cos\alpha + \frac{1}{4} K_{in} \sin^2 2(\beta - \alpha), \quad (3)$$

where μ_0 is the permeability of vacuum and M_s is saturation magnetization. The equilibrium direction of \mathbf{M}_s is determined by $\partial F_{in}/\partial\alpha = 0$, that is

$$h \sin\alpha - \frac{1}{4} \sin 4(\beta - \alpha) = 0, \quad (4)$$

where the reduced field $h = H/H_a^{in}$, the in-plane anisotropic field $H_a^{in} = 2K_{in}/\mu_0 M_s$. When $\beta = 45^\circ$, Eq. (4) changes to

$$2\cos^3\alpha - \cos\alpha - h = 0. \quad (5)$$

Fig. 1(c) can be well fitted by Eq. (5) with $H_a^{in} = 90$ mT. The value $H_a^{in} = 90$ mT can be directly obtained from the point where M deviates from M_s shown in Fig. 1(c), which is corresponding to the condition of $\cos\alpha = 1$ and $h = 1$ described by Eq. (5). The well-fitting clearly shows the magnetization from hard axis to easy axis is a rotation process with a remanence $\cos 45^\circ$.

For the situation of out-of-plane, we introduced the Zeeman energy, the demagnetization energy and the out-of-plane uniaxial anisotropy

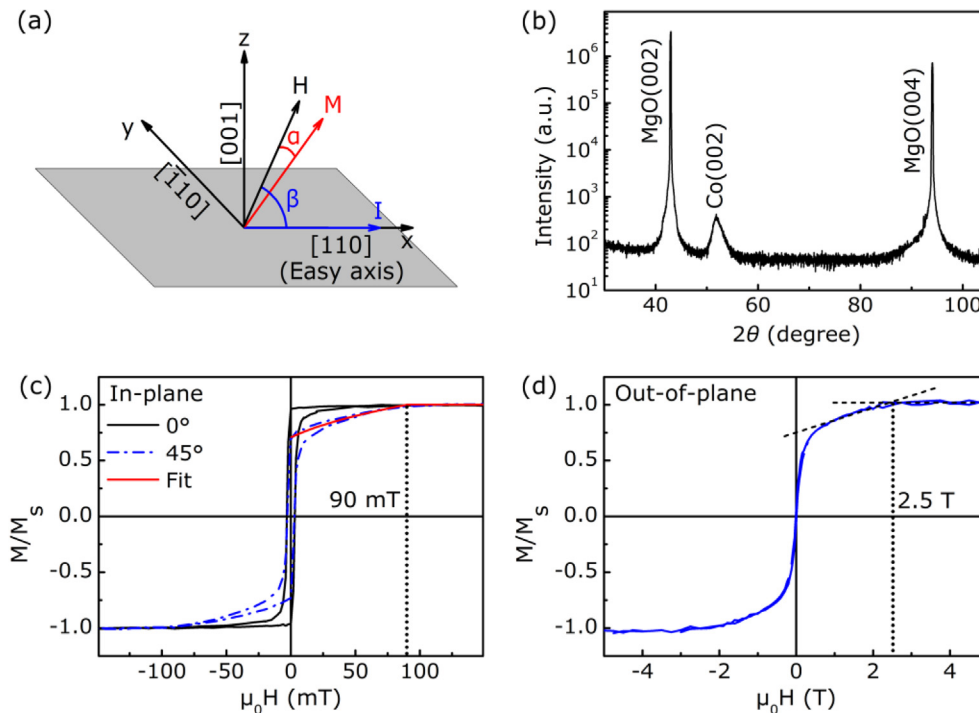


Fig. 1. Characterization results of the Co/MgO thin films. (a) Measurement schematic of the ADMR. (b) X-ray diffraction pattern of θ - 2θ scans. Hysteresis loops (c) at easy (0°) and hard (45°) axes for in-plane and (d) out-of-plane configuration at room temperature. The red solid line is the fitted curve by Eq. (5).

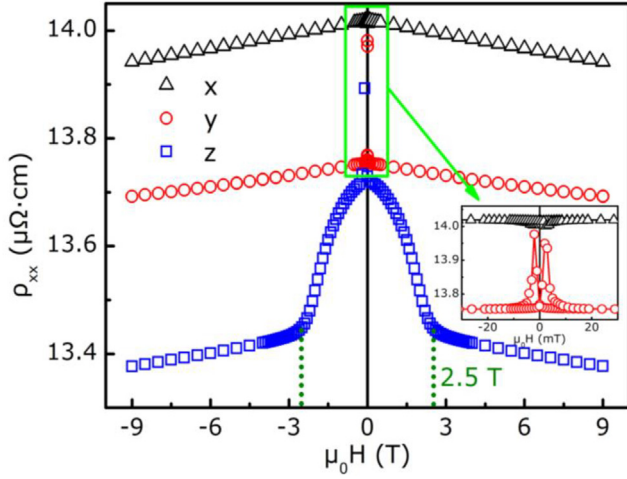


Fig. 2. Magnetoconductance as a function of magnetic field applied along the x , y , and z axes, respectively. The partially enlarged curves of magnetoconductance along x and y axes are shown in inset figure.

energy characterized by a constant K_{out} , and the total free energy density is expressed as [29–31]

$$F_{out} = -\mu_0 M_s H \cos\alpha + \frac{1}{2} \mu_0 M_s^2 \sin^2(\beta - \alpha) + K_{out} \sin^2(\beta - \alpha), \quad (6)$$

the equilibrium direction of magnetization is determined by

$$h \sin\alpha - \frac{1}{2} \sin 2(\beta - \alpha) = 0, \quad (7)$$

where the reduced field $h = H/H_a^{out}$, the effective out-of-plane anisotropic field $H_a^{out} = (M_s + 2K_{out}/\mu_0 M_s)$. It is found that when $\beta = 90^\circ$ the solutions of Eq. (7) are $\cos\alpha = h$ and $\sin\alpha = 0$. Then $H_a^{out} = 2.5$ T can be obtained from the turning point $h = 1$ in the hysteresis loop shown in Fig. 1(d).

In Fig. 2, we present field-dependent magnetoconductance along the three main axes x (easy axis), y (easy axis) and z (hard axis), respectively. Compared with the hysteresis loops shown in Fig. 1(c) and (d), under low applied magnetic field (such as $H < 20$ mT in-plane), magnetoconductance shows complex variation trend the same as magnetization. It caused by domain wall nucleation and propagation as mentioned above. But when H is high enough or even larger than H_a , magnetoconductance declines linearly to guarantee a true single-domain rotation [23,24]. Thus, it further proves the availability of coherent rotation mechanism in the range of field that we research.

3.2. Out-of-plane ADMR

As shown in Fig. 3(a), we measured the out-of-plane ADMR under different magnetic fields in xz plane. We can clearly see that curves do not satisfy the relationship of $\cos^2\beta$. Even if the field reaches 8.75 T, the full width at half maximum of peak region ($\beta = 180^\circ$) is about 30° larger than that of the valley region ($\beta = 90^\circ$). The fitting result of the ADMR by $\cos^2\beta$ under 5 T shown in Fig. 3(b) has significantly deviated from the experimental data especially around 45° . This indicates that there is a significant deviation of \mathbf{M} from \mathbf{H} even H is larger than the anisotropic field H_a^{out} [24].

It is known that magnetization \mathbf{M} of a single-domain particle can never be completely magnetized to the direction of \mathbf{H} except for easy and hard axes within the coherent rotation mechanism. According to the Stoner-Wohlfarth model [22], the simplest anisotropic free energy density is consistent with the Zeeman energy $-\mu_0 M_s H \cos\alpha$ and the uniaxial anisotropy energy $K \sin^2(\beta - \alpha)$. The equilibrium direction of magnetization is determined by

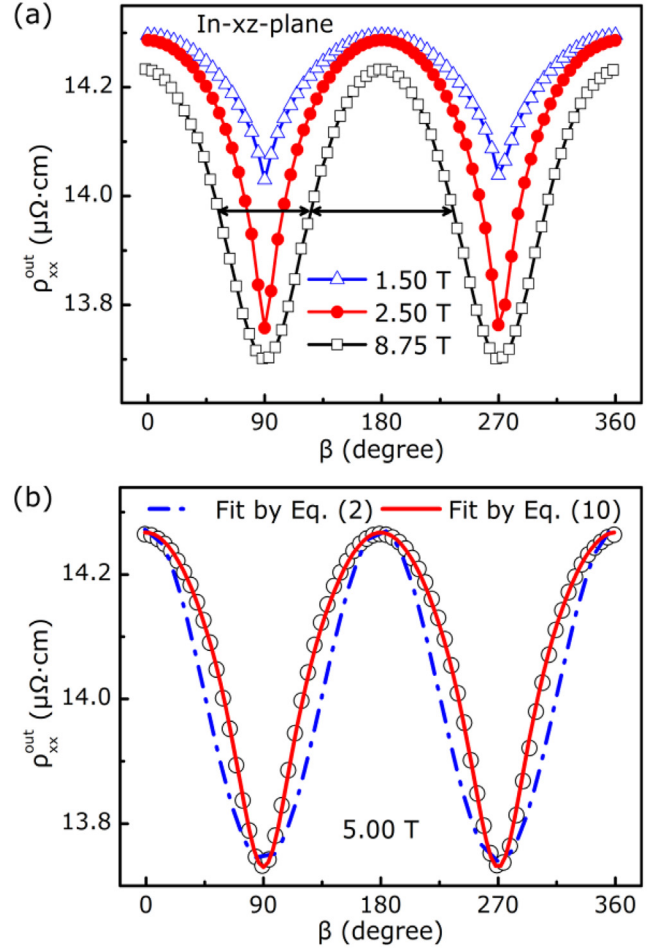


Fig. 3. (a) ADMR curves under different magnetic fields in xz -plane. (b) ADMR under 5 T for out-of-plane configuration. The black open circle is the experimental data. The red solid line is the fitted curve by Eq. (10), and the blue dash dotted line is the fitted curve by Eq. (2).

$$\beta - \alpha = \frac{1}{2} \arcsin(2h \sin\alpha), \quad (8)$$

where $h = H/H_K$, $H_K = 2K/\mu_0 M_s$. Within the magnetization region, $\alpha \leq \beta \leq 90^\circ$, the arcsine function indicates the value of α decreases with increasing h . The maximum values of $\alpha = 30.0^\circ$, 14.5° and 9.6° occur at $\beta = 75.0^\circ$, 59.5° and 54.5° when $h = 1, 2$ and 3 . Therefore, we had to consider the deviation of \mathbf{M} from \mathbf{H} about the out-of-plane ADMR.

We use the small angle α approximation to obtain an analytical expression of α , which is still missing for Eq. (7). By using the Taylor series at $\alpha = 0$, we got an approximate expression

$$\alpha \approx \frac{\sin 2\beta}{2(h + \cos 2\beta)}. \quad (9)$$

Combining Eqs. (9) and (1), we obtained an appropriate phenomenological formula of out-of-plane ADMR under the small-angle approximation,

$$\rho_{xx}^{out} \approx \rho_p + (\rho_{\parallel} - \rho_p) \cos^2 \left(\beta - \frac{\sin 2\beta}{2(h + \cos 2\beta)} \right), \quad (10)$$

where ρ_p is the resistivity out-of-plane with magnetization aligned along z axis [32]. The fitting results by Eq. (10) shown in Fig. 3(b) are coincident with the original data when the anisotropic field $H_a^{out} = 2.7$ T. The magnitude of H_a^{out} is close to the result 2.5 T obtained by the hysteresis loop shown in Fig. 1(d).

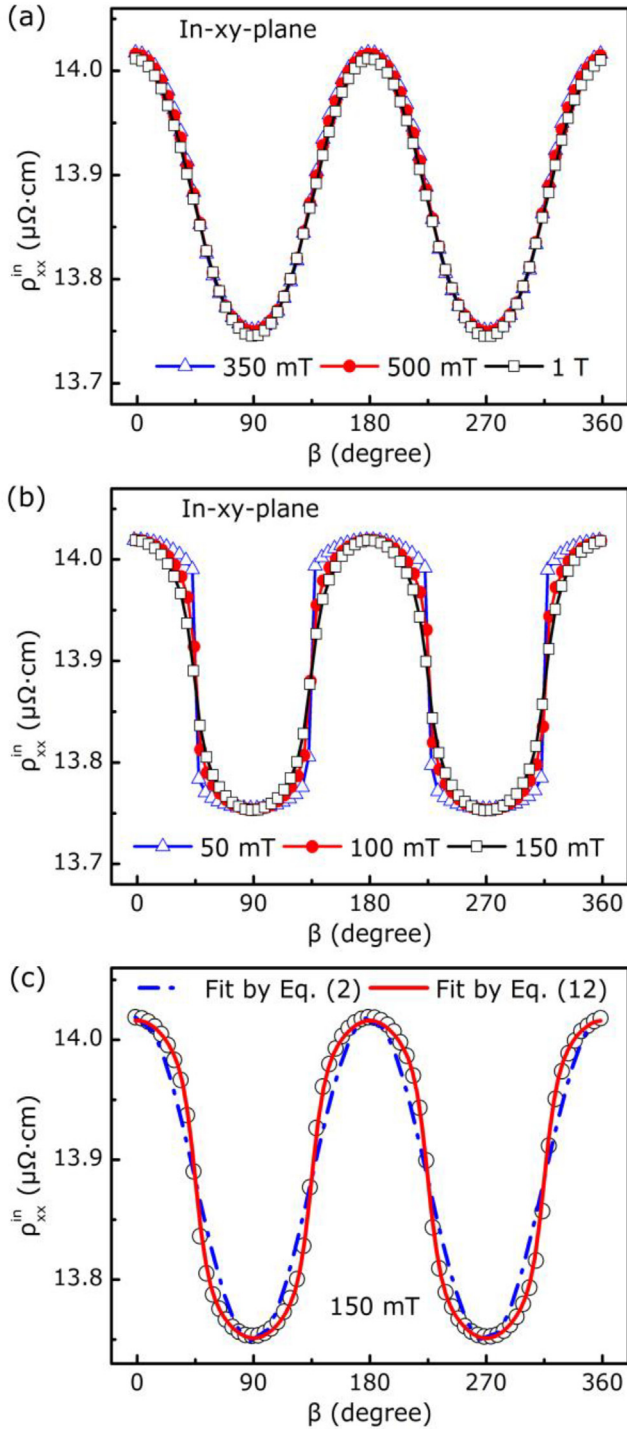


Fig. 4. ADMR curves under different fields which are (a) larger than the anisotropic field and (b) close to the anisotropic field in *xy*-plane. (c) ADMR under 150 mT for in-plane configuration. The black open circle is the experimental data. The red solid line is the fitted curve by Eq. (12), and the blue dash dotted line is the fitted curve by Eq. (2).

3.3. In-plane ADMR

The results of the ADMR curves measured in-plane are shown in Fig. 4. It was found that the ADMR curves shown in Fig. 4(a) look like a cosine function when the field is much larger than the in-plane anisotropic field 90 mT, i.e. 350 mT, 500 mT, and 1 T. But the ADMR curves shown in Fig. 4(b) have significantly deviated from the cosine function especially between 22.5° and 45° for the field at 50 mT, 100 mT, and

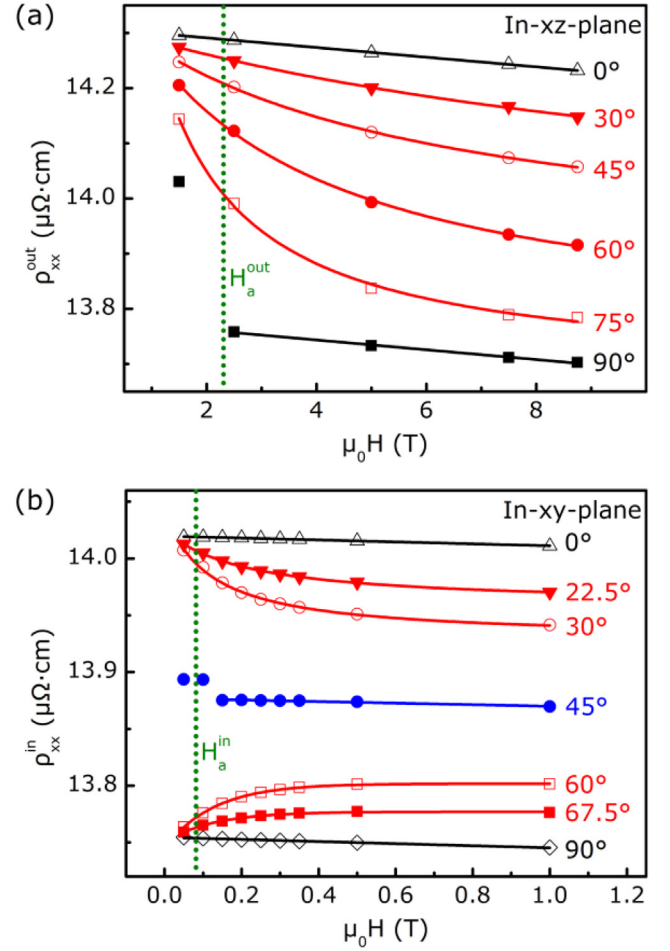


Fig. 5. Field-dependent ADMR at several selected typical β values (a) in *xz*-plane and (b) in *xy*-plane.

150 mT, which are close to the in-plane anisotropic field.

To show the deviate of the ADMR induced by \mathbf{M} from the $\cos^2\beta$ function, we used Taylor's series for Eq. (4) at $\alpha = 0$, and obtained a similar result as follow:

$$\alpha \approx \frac{\sin 4\beta}{4(h + \cos 4\beta)}. \quad (11)$$

Therefore, the in-plane ADMR formula under the small-angle approximation is

$$\rho_{xx}^{in} \approx \rho_t + (\rho_{||} - \rho_t) \cos^2 \left(\beta - \frac{\sin 4\beta}{4(h + \cos 4\beta)} \right), \quad (12)$$

where ρ_t is instead by ρ_l in-plane [32]. The experimental data measured at 150 mT are well fitted by Eq. (12) with $H_a^{in} = 88$ mT shown in Fig. 4(c). The magnitude of H_a^{in} is approach to 90 mT obtained by the hysteresis loops shown in Fig. 1(c).

3.4. Non- $\cos^2\beta$ nature

Fig. 5 presents the field-dependent ADMR at several typical β values in out-of-plane and in-plane geometry. For both out-of-plane and in-plane configurations, the ADMR varies linearly with H when H is larger than the anisotropic field at easy or hard axis. The slowly linear decreasing comes from the spin-magnon scattering [33]. When H deviates from the direction of easy and hard axes, the ADMR approach infinitely certain values at different β . The nonlinear changes are more obvious at 45° for out-of-plane configuration and 22.5° to 45° for in-plane configuration, which is consistent with the significant deviation of

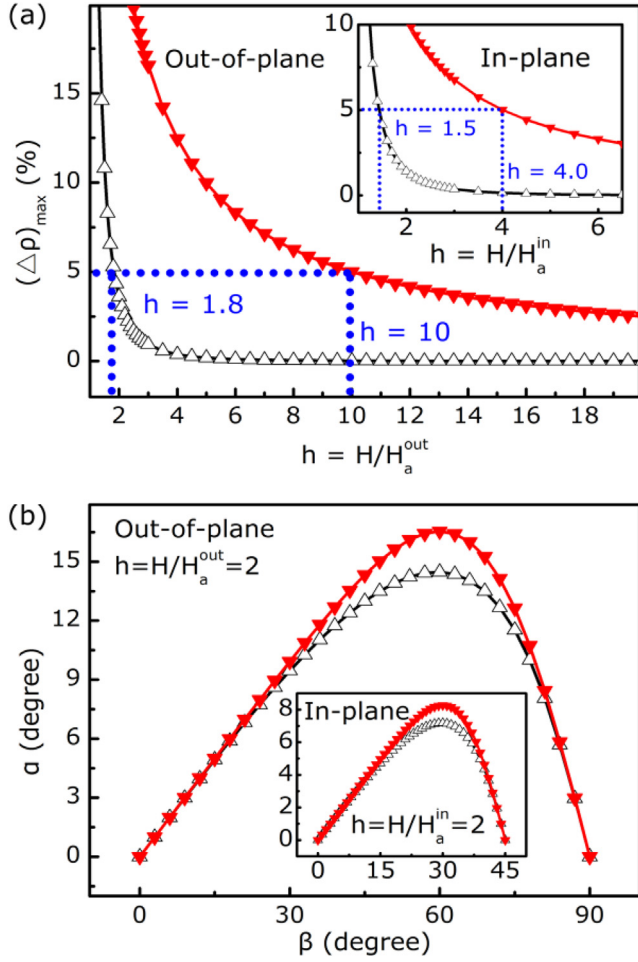


Fig. 6. (a) Error comparison of small angle approximate and traditional saturation sense magnetoresistance for out-of-plane configuration. The black open triangles represent the maximum error of approximate resistivity ρ_{xx}^{out} with respect to the accurate numerical resistivity ρ_{xx} . The red solid triangles represent the error of $\cos^2\beta$ fitting. (b) Comparison of the approximate solution and accurate numerical solution of α for out-of-plane configuration. The black open triangles represent the accurate numerical solution of α obtained from Eq. (7). The red solid triangles represent the approximate solution of α by Eq. (9). The insets show the corresponding situation for in-plane configuration.

ADMR at those angles in Fig. 3(a) and 4(b). These results indicate that the non- $\cos^2\beta$ nature of ADMR is that the magnetization can never be strictly saturated except at easy and hard axes.

3.5. Validity of the small angle approximation

In order to find the effective range of the field H under which the Eqs. (10) and (12) are valid, it is necessary to find out the error of the small-angle approximation. It is known that the difference between the angle α obtained from Eqs. (9) or (11) and the accurate numerical result described by Eq. (7) or (4) is related to the strength and direction of the field. For out-of-plane configuration, we defined the normalized error of resistivity $(\Delta\rho)_{max}$ to present the maximum difference between the resistivity ρ_{xx}^{out} and the accurate numerical resistivity ρ_{xx} calculated from Eq. (1) with Eq. (7)

$$(\Delta\rho)_{max} \equiv \frac{(\rho_{xx}^{out} - \rho_{xx})_{max}}{\rho_{\parallel} - \rho_{\perp}} = \left\{ \cos^2 \left[\beta - \frac{\sin 2\beta}{2(h + \cos 2\beta)} \right] - \cos^2(\beta - \alpha) \right\}_{max} \quad (13)$$

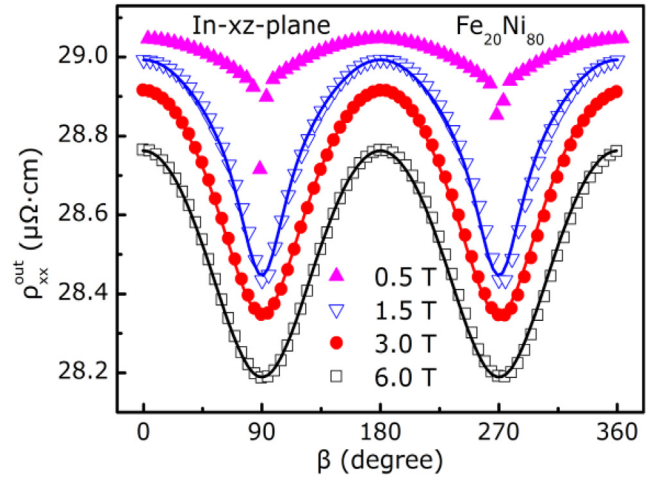


Fig. 7. ADMR of polycrystalline $\text{Fe}_{20}\text{Ni}_{80}$ thin film under different fields in xz -plane. The solid line is the fitted curves by Eq. (10).

Fig. 6(a) shows the relationship between $(\Delta\rho)_{max}$ and h for out-of-plane configuration. It can be seen that $(\Delta\rho)_{max}$ decreases dramatically with increasing h . When h is larger than 1.8, the error is less than 5%. For comparison, Fig. 6(a) also shows the error of $\cos^2\beta$ fitting. It is found that the error is less than 5% when h is larger than 10. Such a large magnetic field is extremely difficult to be obtained in the lab. For in-plane configuration, a similar error curve is shown in the inset of Fig. 6(a). The small-angle approximation is a nice approach to describe the ADMR when h is larger than or equal to 2.

Fig. 6(b) shows the out-of-plane β dependence of α obtained from Eqs. (7) and (9) with $h = 2$. The in-plane results obtained from Eqs. (4) and (11) are presented in the inset of Fig. 6(b). It is found that the deviation of the approximate solution from the accurate solution is less than 2° for both out-of-plane and in-plane configurations. This is the reason that the Eqs. (10) and (12) can well describe ADMR induced by \mathbf{M} when H is larger than or equal to $2H_a$.

To further demonstrate the validity of the Eq. (10), we measured the ADMR of polycrystalline $\text{Fe}_{20}\text{Ni}_{80}$ film under different magnetic fields at room temperature. Fig. 7 shows the similar non- $\cos^2\beta$ characteristic between ρ_{xx}^{out} and β even though H is larger than $2H_a$. By using Eq. (10), the experimental data can be well fitted with anisotropic field $H_a^{out} = 1.0$ T which is dominated by demagnetizing field when $H \geq 1.5$ T, and the error is also less than 5%. Obviously, Eq. (10) are also suitable for polycrystalline samples. As for in-plane configuration, it should be mentioned that the disorder of crystal grains orientation causes the hard axis and the easy axis to be averaged out, and the effect of the demagnetizing field can be ignored. Thus, almost no magnetization deviates from the direction of the applied magnetic field, and Eq. (12) degenerates into Eq. (2).

4. Conclusions

The non- $\cos^2\beta$ ADMR induced by magnetization \mathbf{M} on the Co/MgO thin films were investigated when H is larger than the anisotropic field for both out-of-plane and in-plane configurations. Due to the influence of the anisotropy field, the direction of the magnetization \mathbf{M} can never completely parallel to the direction of \mathbf{H} except at easy and hard axes, which causes a non- $\cos^2\beta$ ADMR. We used the small-angle approximation to obtain the analytical expression of the deviation angle of \mathbf{M} from \mathbf{H} . By error analysis, we demonstrated that the Eqs. (10) and (12) are appropriate to describe ADMR of magnetization when H is larger than $2H_a$ no matter the configuration is out-of-plane or in-plane. The non- $\cos^2\beta$ characteristic is the key to separate ADMR induced by \mathbf{M} from other contributions, which may be used to the ADMR analysis of magnetic topology materials and spintronic devices.

CRediT authorship contribution statement

Yu Miao: Methodology, Conceptualization, Validation, Investigation, Formal analysis, Writing - original draft, Writing - review & editing. **Xiaorui Chen:** Methodology, Investigation, Validation, Writing - original draft, Writing - review & editing. **Shuanglong Yang:** Investigation. **Kun Zheng:** Investigation. **Zhongyuan Lian:** Investigation. **Yongzuo Wang:** Investigation. **Pengju Wang:** Investigation. **Cunxu Gao:** Writing - review & editing. **Dezheng Yang:** Supervision, Validation, Writing - review & editing. **Desheng Xue:** Supervision, Conceptualization, Validation, Writing - review & editing, Funding acquisition, Project administration.

Declaration of Competing Interest

The authors declare that they have no known competing financial interests or personal relationships that could have appeared to influence the work reported in this paper.

Acknowledgments

This work was supported by the National Natural Science Foundation of China (Grant Nos. 11674143, 11674141 and 11774139) and PCSIRT (Grant No. IRT 16R35).

References

- [1] T.R. McGuire, J.A. Aboaf, E. Kloholm, *IEEE Trans. Magn.* 20 (1984) 972.
- [2] R. Ramos, S.K. Arora, I.V. Shvets, *Phys. Rev. B* 78 (2008) 214402.
- [3] M. Tsunoda, H. Takahashi, S. Kokado, Y. Komazaki, A. Sakuma, M. Takahashi, *Appl. Phys. Express* 3 (2010) 113003.
- [4] F.J. Yang, Y. Sakuraba, S. Kokado, Y. Kota, A. Sakuma, K. Takanashi, *Phys. Rev. B* 86 (2012) 020409.
- [5] S. Kokado, M. Tsunoda, K. Harigaya, A. Sakuma, *J. Phys. Soc. Jpn.* 81 (2012) 024705.
- [6] H. Nakayama, M. Althammer, Y.-T. Chen, K. Uchida, Y. Kajiwara, D. Kikuchi, T. Ohtani, S. Geprags, M. Opel, S. Takahashi, R. Gross, G.E.W. Bauer, S.T.B. Goennenwein, E. Saitoh, *Phys. Rev. Lett.* 110 (2013) 206601.
- [7] S. Nandy, G. Sharma, A. Taraphder, S. Tewari, *Phys. Rev. Lett.* 119 (2017) 176804.
- [8] D. Ma, H. Jiang, H. Liu, X.C. Xie, *Phys. Rev. B* 99 (2019) 115121.
- [9] R. Singha, S. Roy, A. Pariari, B. Satpati, P. Mandal, *Phys. Rev. B* 98 (2018) 081103.
- [10] Q. Liu, F. Fei, B. Chen, X. Bo, B. Wei, S. Zhang, M. Zhang, F. Xie, M. Naveed, X. Wan, F. Song, B. Wang, *Phys. Rev. B* 99 (2019) 155119.
- [11] S. Zhang, Q. Wu, Y. Liu, O.V. Yazyev, *Phys. Rev. B* 99 (2019) 035142.
- [12] N.J. Ghimire, M.A. Khan, A.S. Botana, J.S. Jiang, J.F. Mitchell, *Phys. Rev. Mater.* 2 (2018) 081201.
- [13] A. Collaudin, B. Fauqué, Y. Fuseya, W. Kang, K. Behnia, *Phys. Rev. X* 5 (2015) 021022.
- [14] G. Xu, Z. Hou, Y. Wang, X. Zhang, H. Zhang, E. Liu, X. Xi, F. Xu, G. Wu, X.-X. Zhang, W. Wang, *J. Phys.: Condens. Matter* 29 (2017) 195501.
- [15] W. Wang, et al., *Nature Nanotech.* 14 (2019) 819.
- [16] Q. Xu, E. Liu, W. Shi, L. Muechler, J. Gayles, C. Felser, Y. Sun, *Phys. Rev. B* 97 (2018) 235416.
- [17] H. Liu, T. Skeren, A. Volodin, K. Temst, A. Vantomme, C. Van Haesendonck, *Phys. Rev. B* 91 (2015) 104403.
- [18] T.R. McGuire, R.I. Potter, *IEEE Trans. Magn.* 11 (1975) 1018.
- [19] D. Wu, P. Wei, E. Johnston-Halperin, D.D. Awschalom, J. Shi, *Phys. Rev. B* 77 (2008) 125320.
- [20] N. Eden, G. Kopnov, S. Fraenkel, M. Goldstein, A. Gerber, *Phys. Rev. B* 99 (2019) 064432.
- [21] K. Pappert, C. Gould, M. Sawicki, J. Wenisch, K. Brunner, G. Schmidt, L.W. Molenkamp, *New J. Phys.* 9 (2007) 354.
- [22] E.C. Stoner, E.P. Wohlfarth, *Philos. Trans. R. Soc. Ser. A* 240 (1948) 599.
- [23] B. Hu, W. He, J. Ye, J. Tang, Y.-S. Zhang, S.S. Ahmad, X.-Q. Zhang, Z.-H. Cheng, *Sci. Rep.* 5 (2015) 14114.
- [24] J. Ye, W. He, Q. Wu, H.-L. Liu, X.-Q. Zhang, Z.-Y. Chen, Z.-H. Cheng, *Sci. Rep.* 3 (2013) 2148.
- [25] O. Benamara, E. Snoeck, T. Blon, M. Respaud, *J. Cryst. Growth* 312 (2010) 1636.
- [26] I.I. Pronin, D.A. Valdaitsev, A.S. Voronchikhin, M.V. Gomoyunova, S.F. Contri, S. Benedetti, P. Lukes, S. Valeri, *Tech. Phys. Lett.* 31 (2005) 494.
- [27] Y. Nukaga, M. Ohtake, O. Yabuhara, F. Kirino, M. Futamoto, *J. Magn. Soc. Jpn.* 34 (2010) 508.
- [28] Q.F. Zhan, S. Vandezande, C. Van Haesendonck, K. Temst, *Appl. Phys. Lett.* 91 (2007) 122510.
- [29] S. Lee, S. Grudichak, J. Sklenar, C.C. Tsai, M. Jang, Q. Yang, H. Zhang, J.B. Ketterson, *J. Appl. Phys.* 120 (2016) 033905.
- [30] A.J. Lee, J.T. Brangham, Y. Cheng, S.P. White, W.T. Ruane, B.D. Esser, D.W. McComb, P.C. Hammel, F. Yang, *Nat. Commun.* 8 (2017) 234.
- [31] J. Oh, L. Humbard, V. Humbert, J. Sklenar, N. Mason, *AIP Adv.* 9 (2019) 045016.
- [32] L.K. Zou, Y. Zhang, L. Gu, J.W. Cai, L. Sun, *Phys. Rev. B* 93 (2016) 075309.
- [33] Y. Kachlon, N. Kurzweil, A. Sharoni, *J. Appl. Phys.* 115 (2014) 173911.